High-Resolution, Submicron Particle Size Distribution Analysis Using Gravitational-Sweep Sedimentation

Walter Mächtle
Polymer Research Laboratory, BASF Aktiengesellschaft, D-67056 Ludwigshafen, Germany

ABSTRACT Sedimentation velocity is a powerful tool for the analysis of complex solutions of macromolecules. However, sample turbidity imposes an upper limit to the size of molecular complexes currently amenable to such analysis. Furthermore, the breadth of the particle size distribution, combined with possible variations in the density of different particles, makes it difficult to analyze extremely complex mixtures. These same problems are faced in the polymer industry, where dispersions of latices, pigments, lacquers, and emulsions must be characterized. There is a rich history of methods developed for the polymer industry finding use in the biochemical sciences. Two such methods are presented. These use analytical ultracentrifugation to determine the density and size distributions for submicron-sized particles. Both methods rely on Stokes' equations to estimate particle size and density, whereas turbidity, corrected using Mie's theory, provides the concentration measurement. The first method uses the sedimentation time in dispersion media of different densities to evaluate the particle density and size distribution. This method works provided the sample is chemically homogeneous. The second method splices together data gathered at different sample concentrations, thus permitting the high-resolution determination of the size distribution of particle diameters ranging from 10 to 3000 nm. By increasing the rotor speed exponentially from 0 to 40,000 rpm over a 1-h period, size distributions may be measured for extremely broadly distributed dispersions. Presented here is a short history of particle size distribution analysis using the ultracentrifuge, along with a description of the newest experimental methods. Several applications of the methods are provided that demonstrate the breadth of its utility, including extensions to samples containing nonspherical and chromophoric particles.

INTRODUCTION

The particle size distribution (PSD) of aqueous dispersions (polymers, dyes, lacquers, pigments, metal sols, etc.) having diameters D between 10 and 3000 nm is one of their most important characteristics. This is also a size range that includes many biological structures. Thus, many of the techniques that have been useful in determining the PSD of other aqueous dispersions are used in biology. Some extant methods include light scattering, chromatography, electron microscopy, sedimentation field-flow fractionation, capillary diffusion fractionation, and ultracentrifugation (UC). The latter method offers the advantages of being versatile, providing high resolution, and being relatively fast (Li et al., 1990). In polymer chemistry, there have been developments in ultracentrifuge-based PSD analysis that might find utility in the biological sciences. Two of these developments are described here that could find use in the pharmaceutical industry and in the analysis of macromolecular and supramolecular structures.

Cantow (1964) first introduced an ultracentrifuge technique to determine the PSD of polymer latices based on Stokes' law. This work improved on that described by Nichols et al. (1932) by taking into account Mie's light-scattering theory of spheres (Mie, 1908). Thereafter, Scholtan and Lange (1972) developed an analogous ultracentrifuge technique that introduced a light-scattering/turbidity detector inside the ultracentrifuge. This method was further developed (Mächtle, 1984) by 1) changing the detection from a single-beam to double-beam arrangement, 2) increasing the experimental throughput by using an eight-cell rotor and multiplexer, and 3) introducing gravitational-sweep protocols in which the rotor speed is increased reproducibly and exponentially from 0 to 40,000 rpm over a 1-h period. The advantage of this gravitational sweep methodology is that samples containing very small particles (~10 nm) can be measured together with samples containing very large particles (~3000 nm), thus eliminating time-consuming test runs to find a proper rotor speed. However, for mixtures of very large particles and very small particles, the PSD is extremely broad, and the standard, single-cell gravitational sweep UC technique fails. This is especially true in cases where the very small particles are only a small fraction of the original mixture.

This failure is caused by the huge difference between the specific turbidities τ/c (Mie's light scattering) of the very small and very large particles. For example, polystyrene particles of 20 and 2000 nm produce τ/c values of 17 and 17,000 cm^2/g, respectively (Heller and Pangonis, 1957). The result is that our usual loading concentration C_s enables the turbidity detector to monitor larger particles properly, whereas the smaller particles are under-represented or overlooked entirely due to the limited range of the detector. To solve this problem we have developed a coupled-PSD technique (Mächtle, 1988), where two samples differing in concentration by 5- to 30-fold are analyzed simultaneously. By splicing together the PSD of these two solutions, it

Received for publication 30 June 1998 and in final form 29 October 1998.
Address reprint requests to Dr. Walter Mächtle, BASF Aktiengesellschaft, Polymer Laboratory, ZKM-G201 Ludwigshafen, Germany. Tel.: 49-0621-6048176; Fax: 49-0621-6092281; E-mail: walter.maechtle@basf-ag.de.

0006-3495/99/02/1080/12 $2.00

is possible to analyze extremely broadly distributed dispersions.

In this paper we first review 1) the physical basis of the UC-PSD measurement, 2) the H_20/D_20-sedimentation analysis (Mächtle, 1984) used to measure both the density distribution and the size distribution of polymer dispersions, and 3) the coupled-PSD technique for the analysis of very broad distributions. The versatility of these different techniques will be demonstrated by several examples. Finally, a new dual-beam turbidity technique will be introduced.

MATERIALS AND METHODS

Experimental setup

Fig. 1 *A* shows a photo of the PSD-determination equipment. It consists of a preparative ultracentrifuge (OPTIMA XL, Spinco, Palo Alto, CA) that has been modified by incorporating the optics and electronics inside the rotor vacuum chamber needed to measure sample turbidity. Fig. 1 *B* shows the laser-detector setup, removed from the vacuum chamber. It consists of a 690-nm laser diode positioned above the rotor and a fast photodiode aligned with it below the rotor. To the right of the rotor is a cell, on top of which is a centerpiece of the type used for turbidity analyses. The centerpiece can be either 3 or 12 mm thick, with a single, sector-shaped sample compartment. The remaining cell components are interchangeable with the schlieren cells used with the model E analytical ultracentrifuge.

A schematic diagram of an apparatus is shown in Fig. 2. The centerpiece is filled with the dispersion to be analyzed. The lower quartz window of each cell has a metallic mask sputter-coated on it. At the center of the window, corresponding to a radius of 6.5 cm, the mask has a slit 2 mm long (tangentially) and 0.2 mm wide (radially). This slit defines the beam used for measuring the light intensity. The intensity I of the light at the detector is reduced from the incident intensity I_{DM} due to light scattering by the particles. The initial concentration of the dispersion is selected so as to yield a starting intensity I_o of approximately 10% of the intensity of light passing through pure dispersant, I_{DM}.

In the case of monodisperse particles, a single sharp boundary is expected for each particle species (Fig. 2), whereas a distribution of species will result in the superposition of several such sharp boundaries, broadening the transition from I_o to I_{DM}. For samples having a broad PSD, fractionation by particle size results in a smeared boundary with large particles running ahead and small particles lagging behind. The intensity record is a broad, continuous transition from I_o to I_{DM} (Fig. 2, solid line). The time it takes a particle to sediment from the meniscus to the detector beam can be used to calculate its diameter D using Stokes' law. Thus, the x axis can be transformed to an absolute diameter. It remains to transform the intensity increment (ΔI_i) into a mass fraction (m_i). This is accomplished by using Mie's theory to adjust the raw turbidity at any time for the particle diameter (Mächtle, 1984). Thus, the value of D calculated from the sedimentation time is needed to transform ΔI_i to m_i. Summing up all m_i values yields the total concentration of the particles.

A schematic diagram of the method is shown in Fig. 3. Seven samples and a reference cell are measured simultaneously, employing a two-beam technique. Signal processing is triggered by the reference cell 0, which is filled with water. The light detector impulses are sized and sorted electronically, digitized for computer processing, and recorded on an eight-channel analog chart recorder as continuous $I(t)$ curves for visual inspection. The turbidity measurement from the seven cells is fully automated. To cover both small particles ($D \approx 10$ nm) as well as very large ones ($D \approx 3000$ nm), the rotor speed is increased exponentially from 0 to 40,000 rpm over the course of an hour. The ability to measure seven cells simultaneously and to raise the rotor speed exponentially is necessary for the two methods described here (Mächtle, 1984, 1988).

Fig. 4 shows the basic relationships used to determine both the particle diameter D and the particle density ρ from Stokes' law. Two snapshots of the distribution from a monodisperse sample of latex particles are shown, one of them taken at the start of the measurement ($t = 0$) and the other one at the time ($t = t_i$) when the particle front has just passed the measuring slit. From consideration of the equilibrium of forces on a particle, the differential equation of its movement may be written. One of this is Stokes' equation (see Fig. 4), which allows the calculation of D_i from the measured sedimentation time t_i if the particle density ρ_{PM} is known. If the particle density is not known, it can be determined by sedimentation in a second dispersant of density ρ_{DM}. As a second medium we employ heavy water, D_2O, having the density 1.10 g/cm^3. With the modified Stokes' equation (Fig. 4, bottom), ρ_{PM} can be determined from the measured sedimentation times in H_2O and D_2O. It should be emphasized that the differential equation in Fig. 4 can be solved for the case $\omega = f(t)$ by substituting $\int \omega^2 dt$, the reduced sedimentation time integral for $\omega^2 t$. This integral is calculated by the computer from measured values of $\omega(t)$.

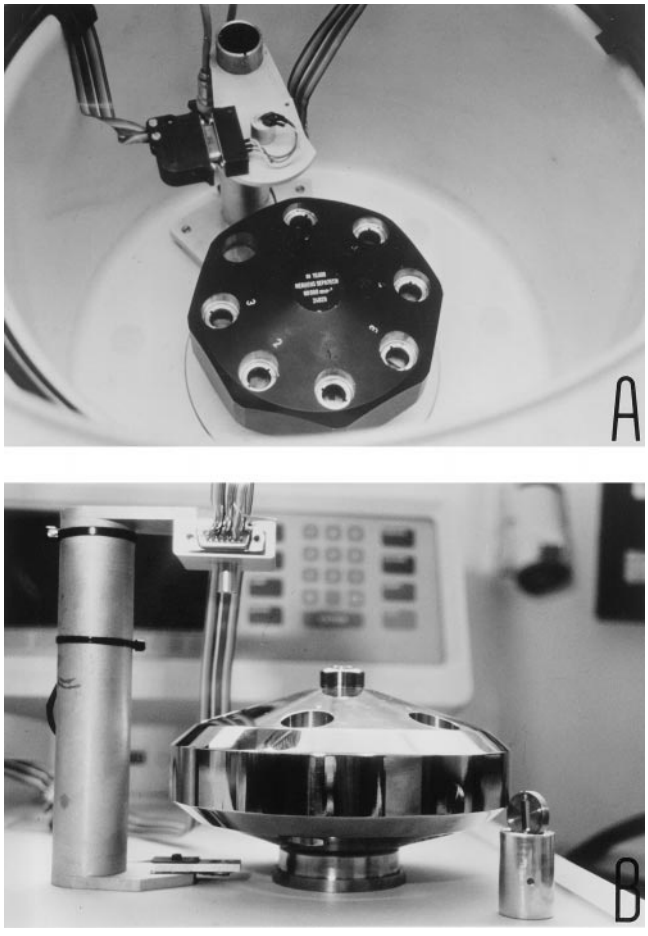

FIGURE 1 (*A*) Vacuum chamber of a preparative UC modified for use in PSD determinations. The eight-hole rotor shown here was custom-made by Heraus. However, the An-50 Ti analytical rotor also could be used. The laser and detector optics are mounted to the vacuum chamber base using a mounting hole used to fasten the heat sink. The rotor can be lifted in and out of the chamber without disturbing the optics. (*B*) Laser-optical setup removed from the chamber. The rotor and a cell also are shown. The configuration is such that in operation the laser diode light source is above the rotor and the photo diode detector is below the rotor. The elliptical laser beam is collimated. A 2 mm × 0.2 mm slit on the bottom window of the cell defines the source beam used for turbidity analysis. As there is very little distance between the slit and the detector, little diffraction broadening of the beam can occur. This arrangement results in a very narrow acceptance angle by the detector, thus ensuring that light scattered at low angles (10°) will be excluded from detection. Thus, effects of stray light are minimized.

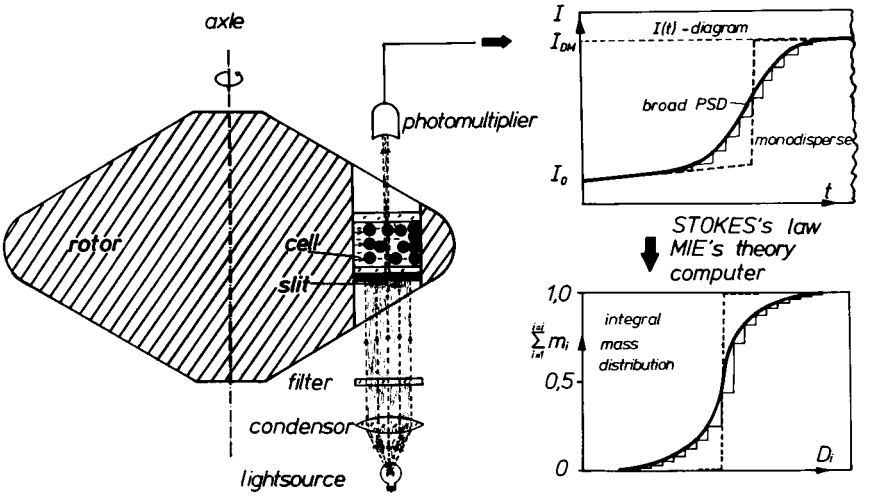

FIGURE 2 Schematic diagram of the measuring apparatus (*left*) and measured distribution curves (*right*). The upper curve presents the intensity of light observed as a function of time from the start of the experiment. The dotted line shows what would be expected for an ideal, monodispersed latex. At early times the intensity slowly increases due to radial dilution. A sharp jump in intensity from I_o to I_D is observed as the boundary passes the detector. For particles of the size analyzed in these sorts of experiments, diffusion broadening of the boundary is negligible.

RESULTS

Example of the gravitational sweep method

An example of the use of the gravitational sweep method is presented in Figs. 5–7. The dispersion in all three graphs consists of a 1 mg/ml mixture of three monodisperse polystyrene calibration latices having diameters of 176, 312, and 794 nm in a mixing ratio of 40:50:10 wt %. Fig. 5 *A* presents the time dependence of the light intensity ratio for cases where a constant rotor speed (4000 rpm) is used (solid lines) and when an exponentially increasing gravitational field (dotted lines) is used for analysis. For each case, the results from seven samples, analyzed simultaneously, are shown to give some idea of the reproducibility of the method. It should be noted that the time needed to complete the experiment is roughly halved using the gravitational sweep method.

The correspondence of the data from these two protocols is demonstrated by the coincidence of the solid and dashed lines when the intensity ratios are graphed as a function of $\int\omega^2 t$ (Fig. 5 *B*) instead of as a function of time (Fig. 5 *A*). Small differences due to the different rotor speeds, such as rotor stretching and tipping of the rotation axis, have not been considered and may account for the slight systematic shift in boundary position for the smallest particles. Because the latex particles are chemically homogeneous, we may convert these curves with Stokes and Mie (for mathematical details see Mächtle, 1984, 1988) into PSD curves. This conversion consists of a two-step process, one for converting the time (or $\int\omega^2 dt$) axis to an effective diameter (Fig. 4) and the other for adjusting the change in intensity to reflect the mass concentration in a boundary. The latter adjustment requires the results of the former conversion. That is, at any time $\int\omega^2 dt$, a boundary of spherical particles passing the detector will have a diameter D, and this diameter will be used for adjusting the intensity ratio according to Mie's theory to obtain the mass concentration. The results of such conversions are seen in Fig. 5 *C*, where Σm_i is plotted versus D_i. These PSD curves conform to within 5% with regard to both the known diameters (176, 312, and 794 nm) and the given mass portions (40, 50, and 10%).

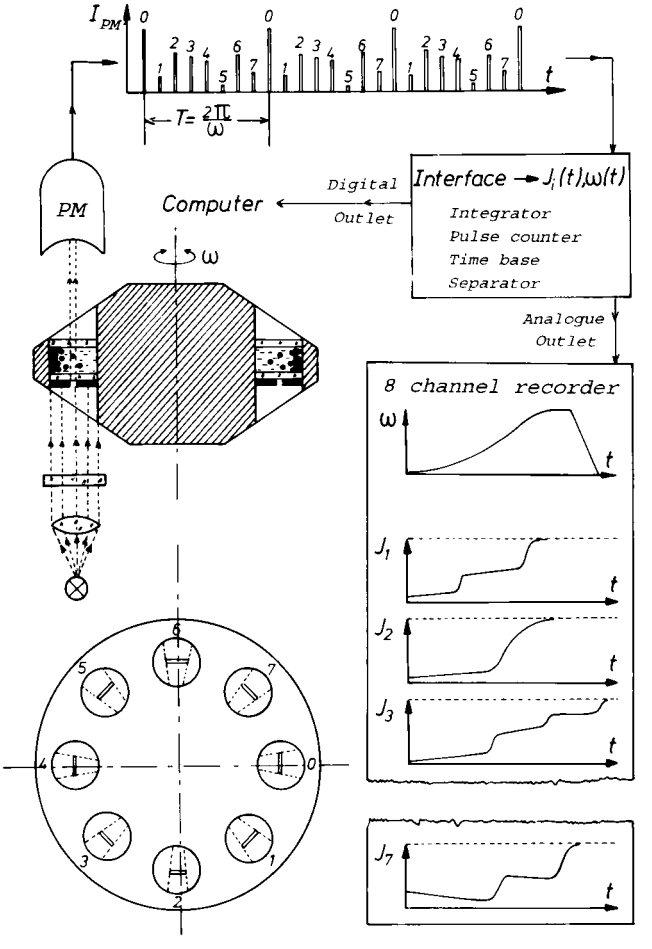

FIGURE 3 Schematic diagram of the PSD-determination method as implemented in the author's laboratory. Signal processing is synchronized to the spinning rotor by the tallest intensity spike, created by filling one cell with water. This intensity also serves as the reference intensity (I_o) used in calculating the turbidity.

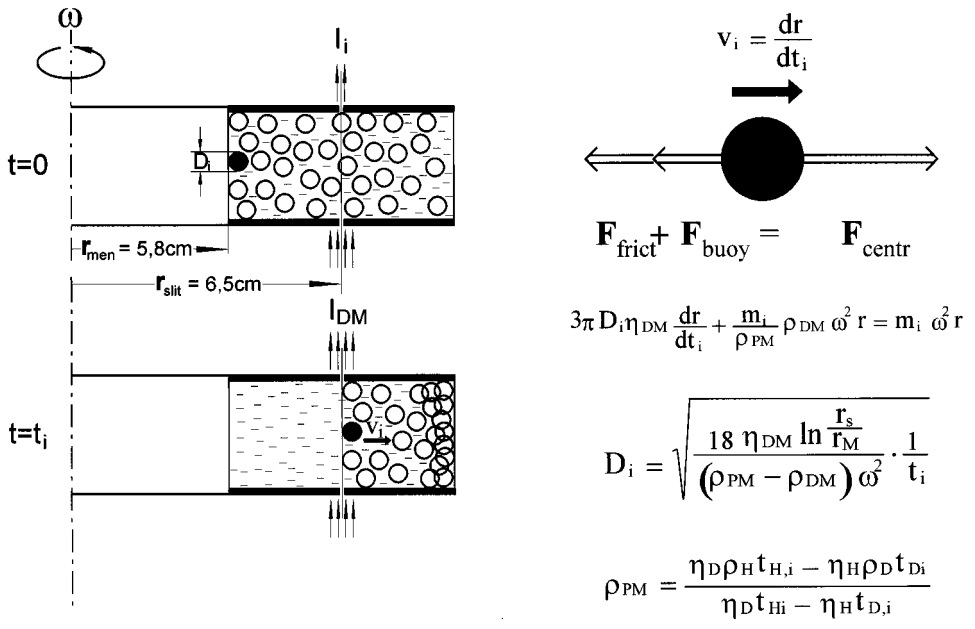

FIGURE 4 Determination of spherical particle diameter D and density ρ_{PM} using Stokes' equation. The balance of forces K_i results in the differential equation shown, which can be solved for the particle diameter if the solvent viscosity η_m, density ρ_{DM}, and particle density ρ_{PM} are known. The latter can be determined from the difference in sedimentation time in H_2O and D_2O dispersants.

Examples of dual-density sedimentation analysis

The use of gravitational sweep PSD can be extended to the analysis of particles differing in density. If the dispersion is not chemically homogeneous (i.e., the density and the refractive index of the particles are not uniform) the resulting PSD, like that shown in Fig. 5 *C*, would be misinterpreted. To analyze unknown dispersions for their chemical homogeneity we have developed a fast H_2O/D_2O analysis. The density differences of mixtures of these two dispersants is used to fractionate a sample with respect to the sample density. The example shown in Fig. 6 illustrates the results from an H_2O/D_2O analysis of a polystyrene latex in three dispersants having different densities. The choice of H_2O and D_2O as dispersants is convenient in this case. It should be noted, however, that the method outlined here is not restricted to these two dispersants. Rather, all that is required is that the two dispersants differ sufficiently in density for the analysis using the equations given in Fig. 4 to be accurate. In the case where there is sufficient redistribution of components in the dispersant to generate a density gradient during sedimentation, the equations must be modified to incorporate the additional complexities by substituting the appropriate position- and time-dependent functions for the density in place of the constants ρ_H, ρ_D, and η_H, ηD to obtain ρ_{DM}. For the present case, such added complexity can be ignored.

To accomplish the analysis in H_2O and D_2O a concentrated dispersion is diluted at a ratio of approximately 1:1000 by the three dispersants: H_2O (ρ = 1.00 g/cm^3), D_2O (ρ = 1.10 g/cm^3), and a 1:1 mixture of H_2O and D_2O, respectively. The corresponding intensity ratio curves for these three dispersions are measured simultaneously. The 1:1 mixture is needed only to decide whether sedimentation or flotation is occurring in the two pure dispersants (for details see Mächtle, 1984). The example shown in Fig. 6 *A* reveals that the latex particles sediment in H_2O but float in pure D_2O. This is made evident by the slower flotation observed in the 1:1 mixture of H_2O and D_2O. The fact that both flotation and sedimentation can be analyzed shows the generality of the method.

To determine the density distribution function, the computer divides the three $I(t)$ curves into 10 fractions. From the three coupled traveling times ($\int \omega^2 dt$) for each fraction, it calculates the particle density ρ_m and the particle diameter D by means of the two Stokes' equations (from Fig. 4). From the calculations, two tables of values can be generated (right side Fig. 6 *A*), one representing the density distribution and the other providing the PSD. In the case presented in Fig. 6 *A*, ρ_m is constant (1.054 g/cm^3), and the dispersion is a chemically homogeneous, nearly monodisphere polystyrene latex with diameters near 155 nm.

Analysis with the H_2O/D_2O method can be used to determine whether sample heterogeneity exists due to particle size differences or due to particle density differences. Fig. 6 *B* shows the analysis of a dispersion that is markedly bimodal. Because the three coupled $\omega^2(t)$ curves can be superimposed by translation along the t axis, the sample must be chemically homogeneous (i.e., having the same ρ_{PM}). Furthermore, the particle density of 0.89 g/cm^3 suggests the sample is polybutadiene. In this case, the bimodality of the PSD is caused by two components having different diameters, 115 and 350 nm, respectively. Indeed, this dispersion we created by mixing polybutadiene particles of 115 and 350 nm at a ratio of 72:28 wt %.

Cases where the particle sizes are the same but particle densities differ also can be analyzed using the H_2O/D_2O method. Fig. 6 *C* shows an example where the three $I(t)$ curves of an unknown dispersion cannot be superimposed

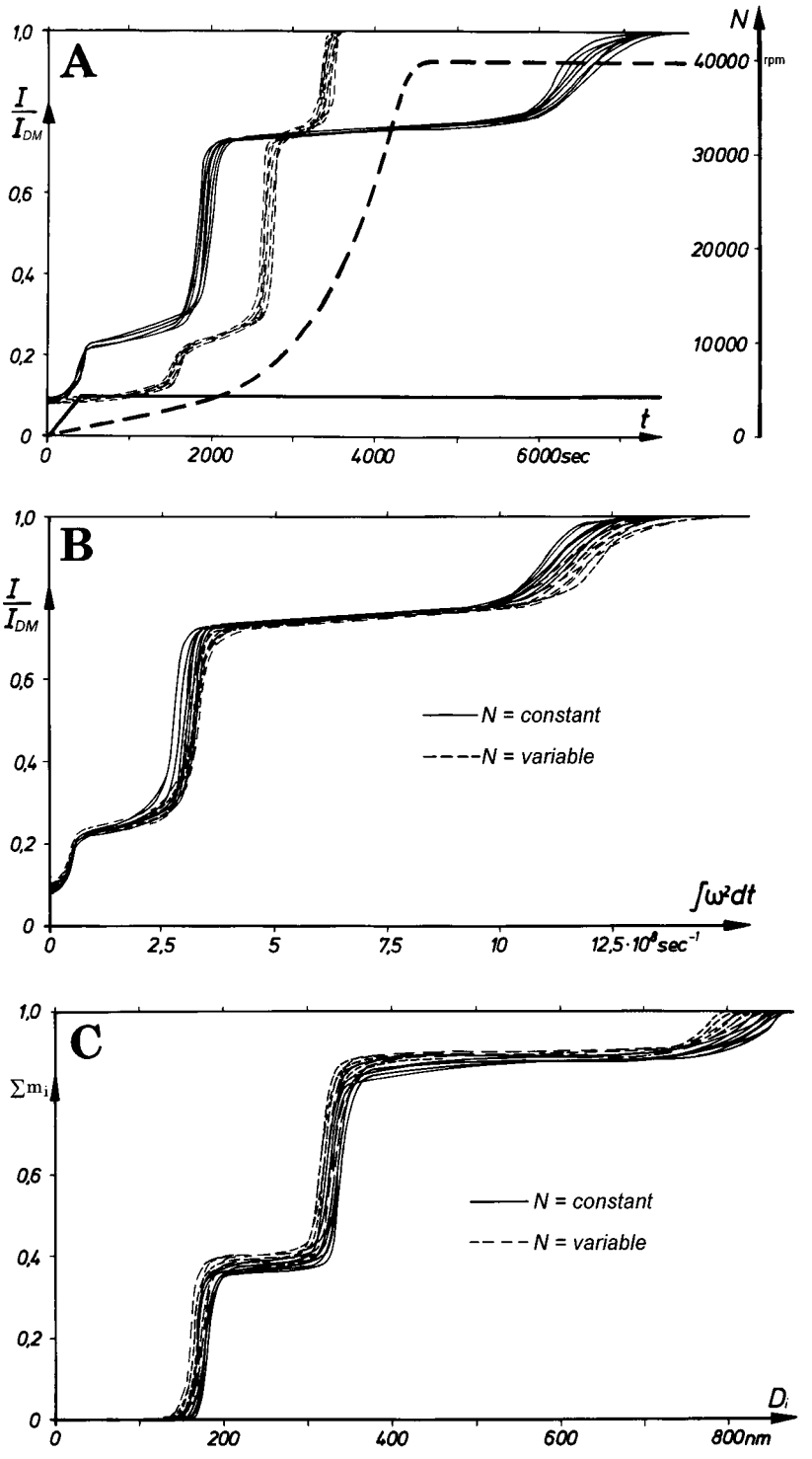

FIGURE 5 (*A*) Intensity ratio curves (transmitted intensity at any time *t* divided by the transmitted intensity for pure dispersant) of seven mixtures of three monodispersed polystyrene calibration latices in water. The time dependence of the rotor speed (*N*) also is shown (*right axis*) for two cases, one for which the rotor speed is constant (——) and one in which the rotor undergoes an exponential acceleration to 40,000 rpm (- - -). The resulting intensity ratio traces for the seven samples for each case are shown. The three boundaries visible in these traces correspond to the time when a boundary of particles passes the detector. Notice that the increase in transmitted light depends on particle size as well as concentration, so that the increase in intensity for the earliest boundary and the latest boundary are nearly equal, even though there is fourfold more material in the latter. Determination of accurate concentrations requires the adjustment of the intensity change to particle diameters using Mie's theory (Mächtle, 1988). (*B*) Regraphing the data in *A* as a function of the integrated sedimentation time ($\int\omega^2 dt$) demonstrates the correspondence of the data obtained using a fixed rotor speed with that obtained using gravitational sweep analysis. (*C*) The resultant mass distribution plot (PSD) for the seven mixtures of three monodispersed polystyrene calibration latices.

by translation along the *t* axis. This means that the sample must be chemically inhomogeneous. Indeed, this dispersion consists of a mixture of polystyrene particles of 155 nm and polybutadiene particles of 115 nm at a ratio of 12:88 wt %. Although these four particles have similar diameters, their densities are quite different. From the H_2O/D_2O analysis, we should be able to determine *D* and ρ_{PM} for each particle type. Each of the 10 factions provides an estimate of ρ and *D*. From the tabulated data, it is clear that some of the ρ and *D* values are reasonable, whereas others (the canceled ones) are physically absurd. Thus, it would seem that it is possible to obtain *C* and *D* from each component in a pauci-disperse sample. At a maximum, H_2O/D_2O analysis provides a rapid check of whether an unknown dispersion is chemically homogeneous or inhomogeneous and thus determines whether a PSD determination by UC is possible or not.

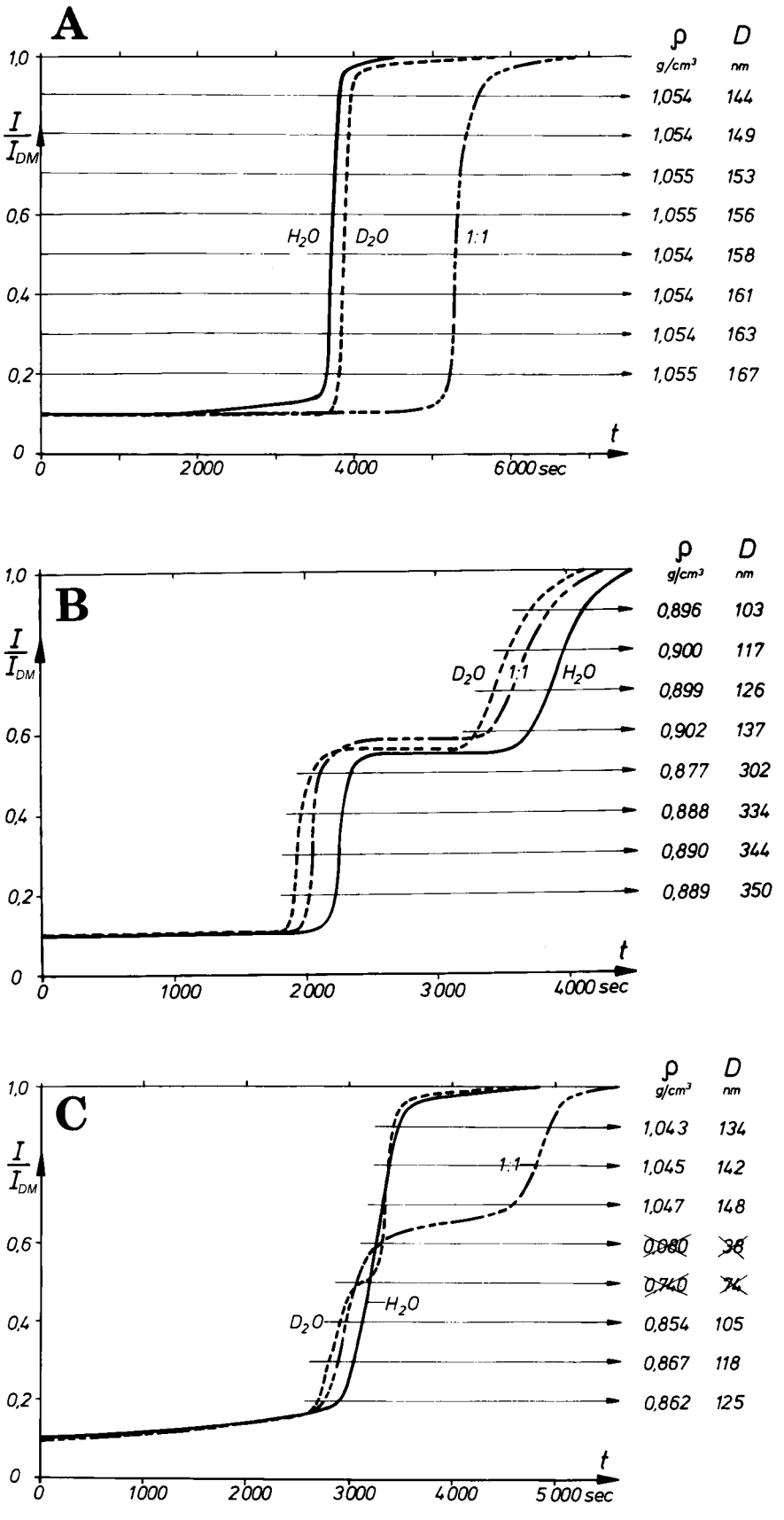

FIGURE 6 (*A*) H_2O/D_2O analysis of a polystyrene latex (D = 155 nm). This sample sediments in H_2O, floats in D_2O, and exhibits slower sedimentation in 1:1 H_2O/D_2O. By combining this information, both the particle size and particle density can be determined. (*B*) H_2O/D_2O analysis of a polybutadiene latex mixture (115 nm + 350 nm). (*C*) H_2O/D_2O analysis of a polystyrene-polybutadiene latex mixture.

Limits of resolution for pauci-disperse chemically homogeneous samples

In an effort to determine how well sedimentation PSD analysis can determine the relative abundance of two dispersants differing somewhat in diameter, mixing experiments were conducted. Fig. 7 *A* shows the $I(t)$ curves of two monodisperse polystyrene calibration latices having diameters of 176 and 220 nm and five mixtures of them at weight ratios of 10:90, 25:75, 50:50, 75:25, and 90:10. As Fig. 7 reveals, the particles are separated unambiguously, even using the gravitational sweep analysis, which has a lower resolution. If constant speed were used, higher resolution would be achieved. Even so, tests like these reveal that it is possible to resolve the times for intensity transitions that differ by ~5%. This seems to be the determining factor in resolving intensities of components for a chemically homogeneous sample. For the example given in Fig. 7 *A*, conversion of the seven $I(t)$ curves into PSD curves yields the result shown in Fig. 7 *B*. For this analysis, the known diameters, as well as the five mixing ratios (marked by arrows), are reproduced to within 5%.

Coupling-PSD technique and measuring examples

Unfractionated samples often are not pauci-disperse but instead contain a broad distribution of particle sizes. To analyze such mixtures, it is necessary to combine the results from samples at different dilutions so that the turbidities of both small and large particles can be measured. This has been accomplished using the so-called coupling-PSD technique. Fig. 8 *A* shows a set of PSD curves for 10 narrowly distributed polystyrene dispersions having $D_{50\%}$ diameters from 67 to 1220 nm. These 10 dispersions were mixed in equal portions of 10 wt % each, thus creating a new dispersion having an extremely broad PSD. Fig. 8 *B* shows the $I(t)$ curve obtained by measuring this mixture of 10 components at the standard concentration of 0.35 g/L (solid

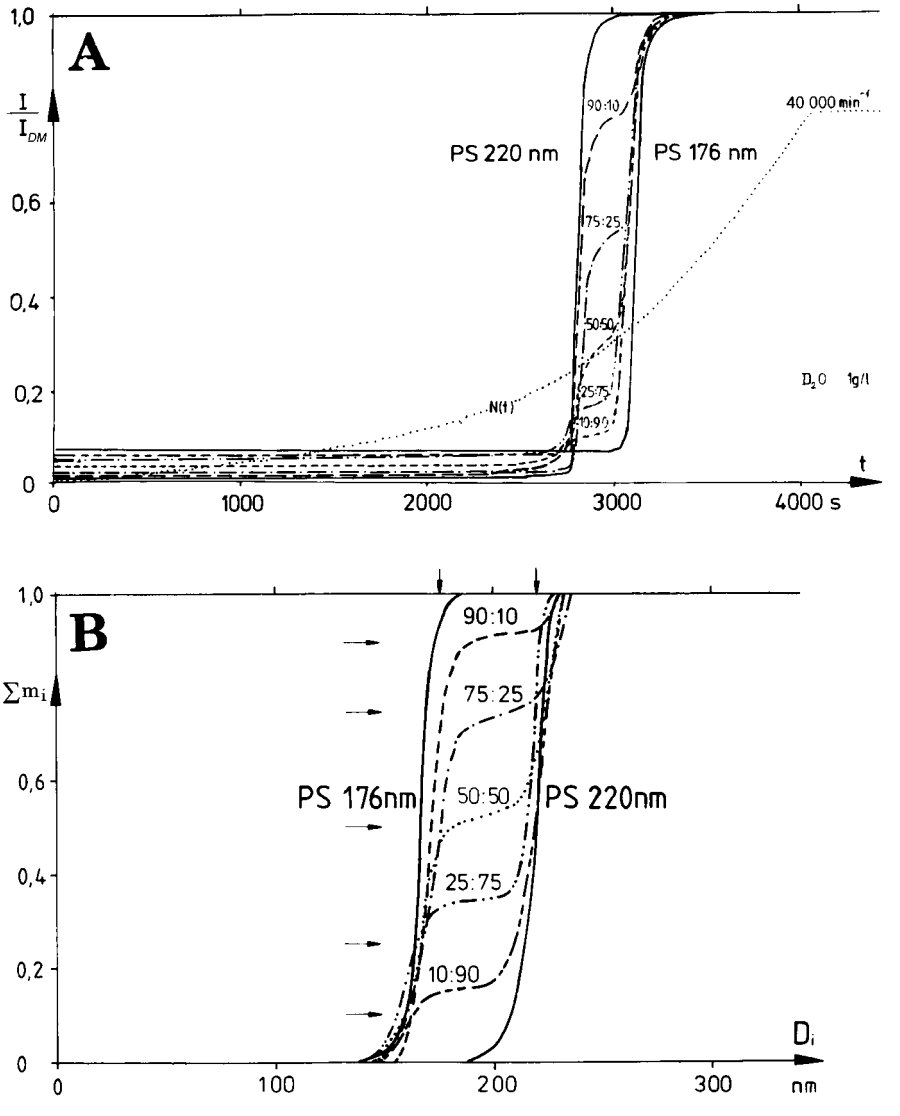

FIGURE 7 (*A*) The resolving power of ultracentrifuge PSD analysis. $I(t)$ curves for seven mixtures of two monodispersed polystyrene calibration latices (176 nm + 220 nm) are shown. ——, intensity curves obtained for the pure components; - - -, results from the different mixtures; · · ·, time dependence of the rotor speed. (*B*) When the data shown in Fig. 11 are transformed according to the Stokes-Mie theory, the resultant PSD curves are produced. ——, the two pure components; - - -, data for the mixtures. The vertical arrows show the radius for each of the components. The horizontal arrows show the known mixing ratios.

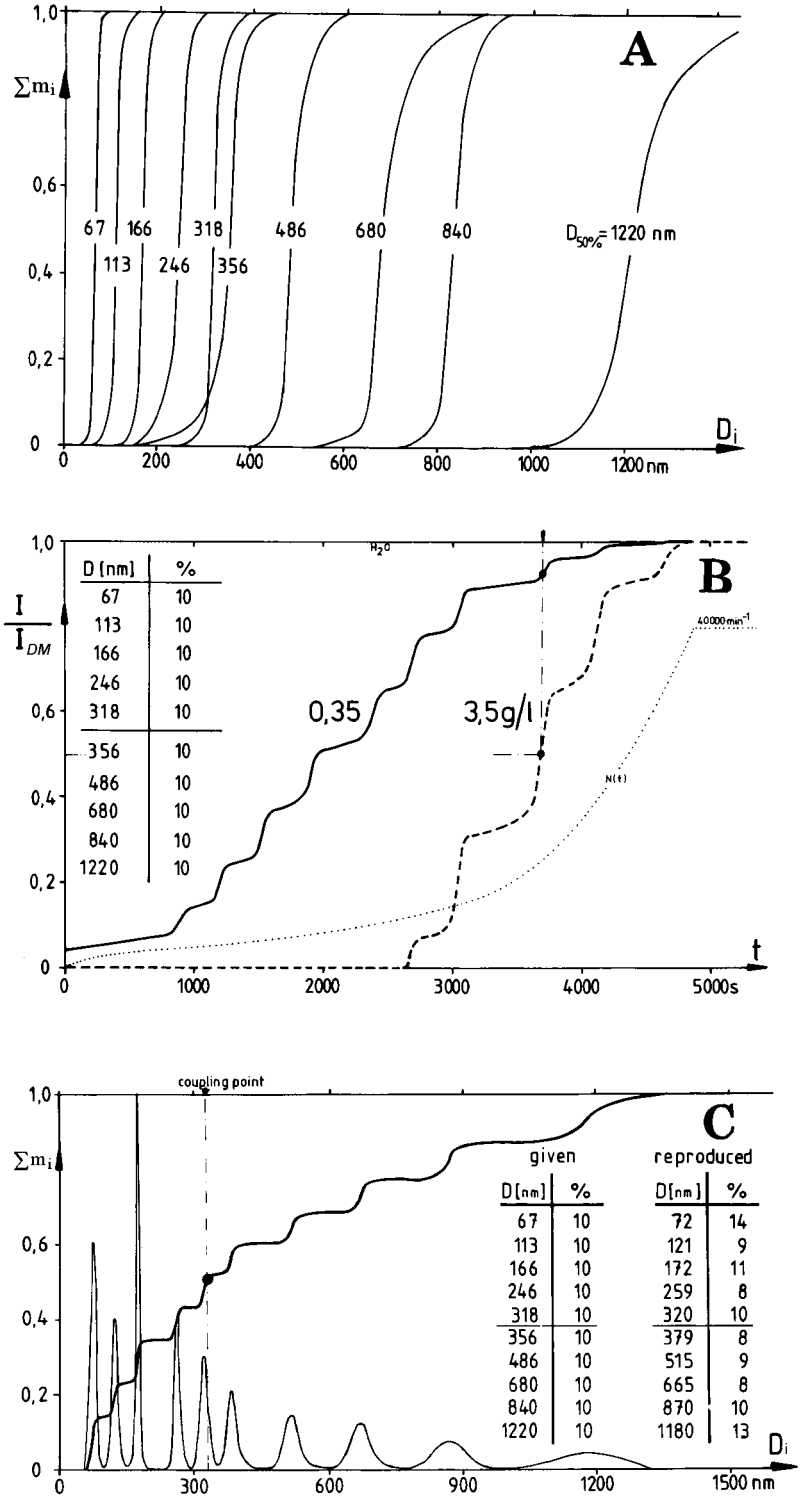

FIGURE 8 (*A*) PSD analysis for 10 different polystyrene latices, each with a narrow size distribution. An equal weight percent mixture of these 10 samples was made to demonstrate the ability of the coupling-PSD technique to resolve broadly distributed mixtures. (*B*) The intensity profiles for a low concentration (0.35 mg/ml, ——) and high concentration (3.5 mg/ml, - - -) analysis of a mixture (equal weight percent) of the 10 latices shown in *A*. · · ·, time dependence of the rotor speed. The arrow and vertical dashed line shows the time point where the two intensity curves were later spliced together. (*C*) Resultant PSD curve for the spliced data shown in *B*. The coupling point where the data from different loading concentrations was spliced together is marked by the vertical dashed line. The integral distribution (*heavy line*) and differential distribution (*light line*) are shown.

line), which results in an initial light intensity of ~5% relative to I_{DM}. Each component can be distinguished clearly as a single step with the exception of component 10, the smallest one. The $I(t)$ step of the latter is tiny because it scatters light relatively weakly. The coupling-PSD technique remedies this by the simultaneous analysis of the 10-component mixture at 0.35 g/L and at a 10-fold higher concentration, i.e., at 3.5 g/L. The second $I(t)$ curve (broken line in Fig. 8 *B*) discloses components 10 through 7 and, partially, component 6. Components 1–5 are not resolved at this higher concentration because their measuring signal is zero (i.e., scattering from component 5 obscures those of 1–4).

The combined results from these two concentrations is obtained from the two $I(t)$ curves by coupling them math-

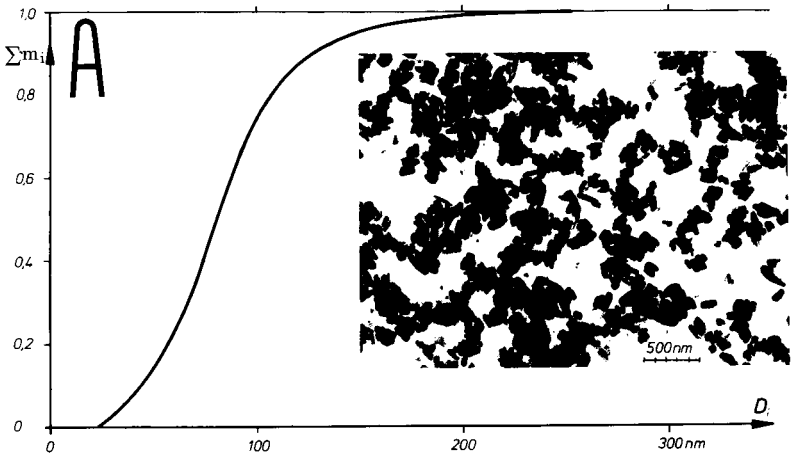

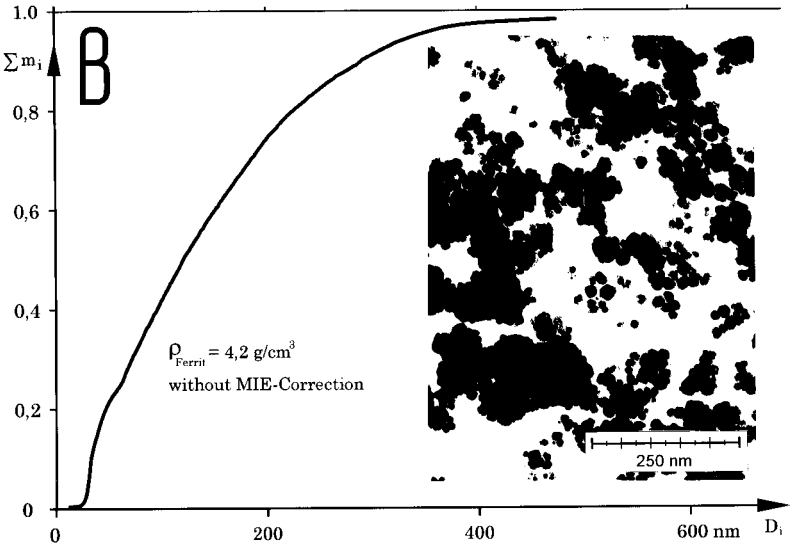

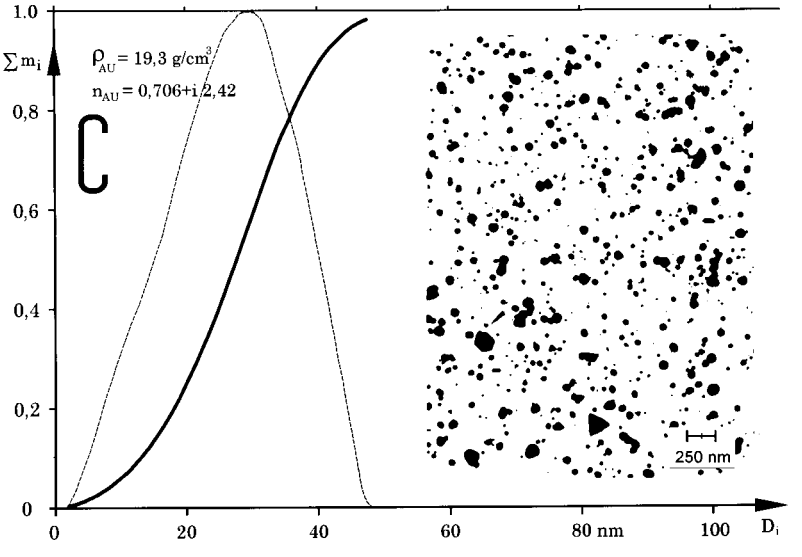

FIGURE 9 (*A*) UC-PSD of a copper-phthalocyanine pigment. (*B*) UC-PSD of Mn/Zn-Ferrite particles in a magnetic fluid, dispersed in H_2O (concentration, 1 g/L). (*C*) UC-PSD of colloid gold particles dispersed in H_2O (concentration, 0.1 g/L).

ematically at the point marked t_κ in Fig. 8 *B*. Thus, the early times of the 0.35 g/L curve is connected to the latter times of the 3.5 g/L curve (for details, see Mächtle, 1988). The coupling of these two curves is dependent on there being minimal effects of concentration on the sedimentation coefficient. For spherical particles, we estimate that the difference in *S* between these two solutions is less than 3% (Rowe, 1992). If we convert this coupled $I(t)$ curve into a PSD curve we obtain the continuous curve shown in Fig. 8 *C*. All 10 components of this dispersion are separated down to the baseline, even the two components of 318 and 356 nm, whose diameters differ by only 12%. The values in the left table of Fig. 8 *C* are the values for the given starting mixture, whereas those in the right table were produced from the analysis. We are able to reproduce the component diameters to within 5% and the weight factors portions of the components to within 15% of their correct values. Thus, the coupling-PSD technique is useful for extremely broadly distributed dispersions.

It should be emphasized that we are able to measure the PSD not only of polymer dispersions but also of pigments, lacquers, and emulsions. In short, the PSD of any kind of dispersed microparticles having diameters in the range from 10 to 3000 nm are amenable to this analysis. The particles do not have to be spherical; other shapes are allowed, too. Light-absorbing particles can be analyzed by this method. This shall be demonstrated by two examples. Fig. 9 *A* shows an electron microscopic image of needle-shaped crystals of a copper-phthalocyanine dye used for printing inks. Also shown is the PSD curve obtained by ultracentrifugation, yielding Stokes equivalent sphere diameters ranging from 30 to 200 nm. Taking the asymmetry of the crystals into account, the size of the particles observed by electron microscopy is in good agreement with that reported by the ultracentrifuge. Serious disagreement between electron microscopic analysis and PSD can be informative. For example, in Fig. 9 *B* is shown a PSD analysis of ferrite particles from a magnetic fluid. The smallest individual particles visible in the electron microscopic image have diameters of ~8–15 nm. These small particles are present in the centrifugal PSD, too. However, the PSD reveals that much larger particles, up to 400 nm, also are present in the fluid. This means that most of the small primary particles are aggregated in the magnetic fluid.

Light-absorbing particles also can be handled by this method by incorporating the appropriate form of Mie's light-scattering theory. For example, the analysis program handles absorbing particles, such as the gold particles in Fig. 9 *C*, which have a complex refractive index (e.g., $n_{Au} = 0.706 - i2.42$ nm at 20°C and $\lambda = 633$ nm). Fig. 9 *C* shows the PSD of colloid gold particles (metal sol) dispersed in H_2O. This sample absorbs light strongly at the wavelength used for analysis. However, all diameters, ranging from 5 to 50 nm, are reproduced by ultracentrifugal PSD and agree well with the diameters determined from the EM analysis. This indicates that the particles in the gold dispersion are not aggregated.

Outlook: new dual-laser-beam technique

The experimental setup with one laser beam, described in Figs. 2–4, has three disadvantages. First, it is not possible to fill the centerpiece cell every time to exactly the same

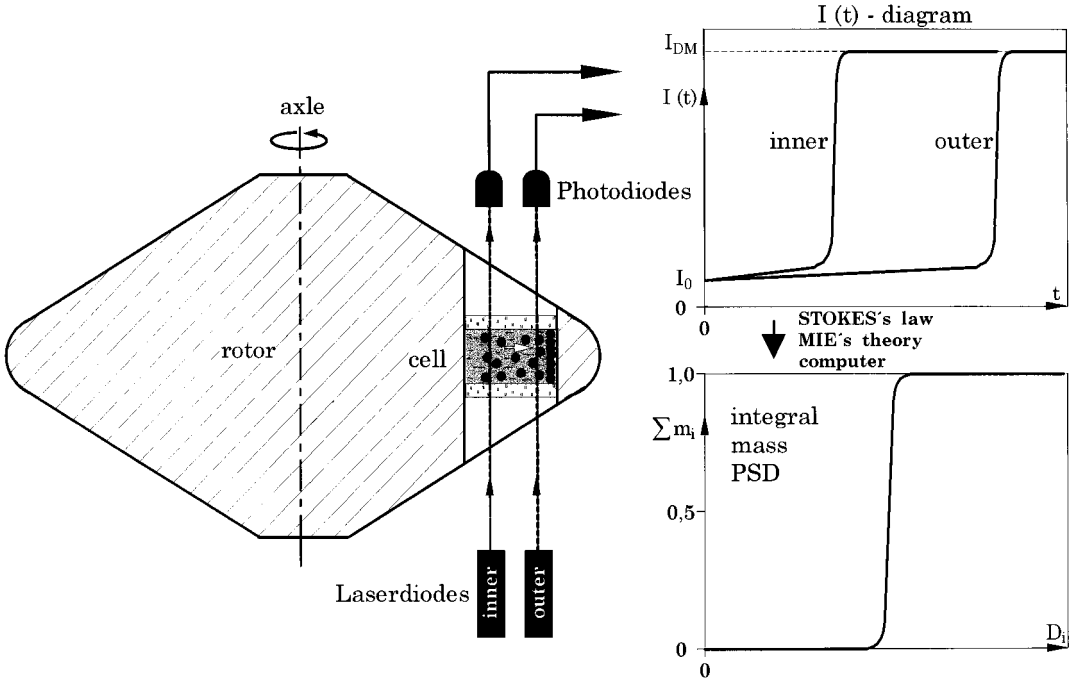

FIGURE 10 Schematic diagram of a two-laser-beam setup in an ultracentrifuge to measure PSD.

height because of small air bubbles of different sizes introduced during the filling process. This results in an error Δr_M in the radius of meniscus r_M (see Fig. 4), which translates to an error in the particle diameter D. Thus, reduction in Δr_M reduces the error in D. Second, the particles of an uncharacterized dispersion may either sediment or float. Thus, the radial position of the laser beam is placed half-way between the meniscus radius r_M and cell bottom r_B. This results in approximately one-half of the maximal possible resolving distance ($r_B - r_M$) being used. Increasing the resolving distance would increase the range diameters that can be measured. Third, in the H_2O/D_2O analysis, a third cell is needed with the dispersion medium composed of a 50:50 mixture of H_2O and D_2O. This is used to decide whether the particles in the dispersion are sedimenting or floating, (i.e., whether r_M or r_B should be used for the starting position of the boundary). If there were no need for this third cell, more H_2O/D_2O analyses could be conducted simultaneously.

To circumvent or minimize these three disadvantages, a new setup, shown in Fig. 10, introduces a second measuring beam. The radial position of the two laser beams, r_1 and r_2, can be varied to anywhere between r_M and r_B. At this time, it is not clear what the optimal position is. The first measurements presented in Fig. 11, *A* and *B*, were done with r_1 at the one-third position and r_2 at the two-thirds position along the distance ($r_B - r_M$).

The graph in Fig. 10 shows a measurement of a monodispersed latex, yielding steep, one-step $I(t)$ fractionation curves for each detector. Both of them and, as a third possibility, the difference of both, deliver, by appropriate Stokes-Mie analysis, a PSD of the latex (if particle density and refractive index are homogeneous and known). The computer decides which of the three PSD curves will provide the highest resolution. For sedimentation, the PSD at r_2 is the best, whereas, in the case of flotation ($\rho_{PM} < \rho_{DM}$), r_1 will provide greater resolution. If r_M is not well known (due to cell-filling error) the difference PSD will be the best one, because the calculation of this PSD does not require knowledge of r_M or r_B. Instead, the value of the new resolving distance ($r_2 - r_1$) is needed. This distance has to be measured only once and is constant for all experiments. Fig. 11, *A* and *B*, shows an example of data acquired with the new two-laser-beam setup.

Fig. 11 *A* presents the two $I(t)$ curves (and the time dependence of the rotor speed) for a 1:1:1 mixture of three monodisperse polystyrene calibration latices having known diameters of 120, 550, and 1300 nm. These two $I(t)$ curves and the difference of both, $I(t)_{inner} - I(t)_{outer}$, are transformed with the Stokes and Mie method into the three PSD curves in Fig. 11 *B*. There is a fairly good agreement between these three PSD curves. The mixing ratio and the diameters are reproduced within ±5%. The small differences between the three PSD curves are under investigation. Early indications are that the difference PSD not only is the most precise but also provides the highest resolution.

Another result is obtained directly from visual inspection of the two $I(t)$ curves: whether a dispersant sediments or floats. If the time needed to reach the outer beam t_{outer} is higher than in the inner beam t_{inner}, the material sediments. Conversely, if $t_{inner} > t_{outer}$, the material floats. A computer can make this decision very easily.

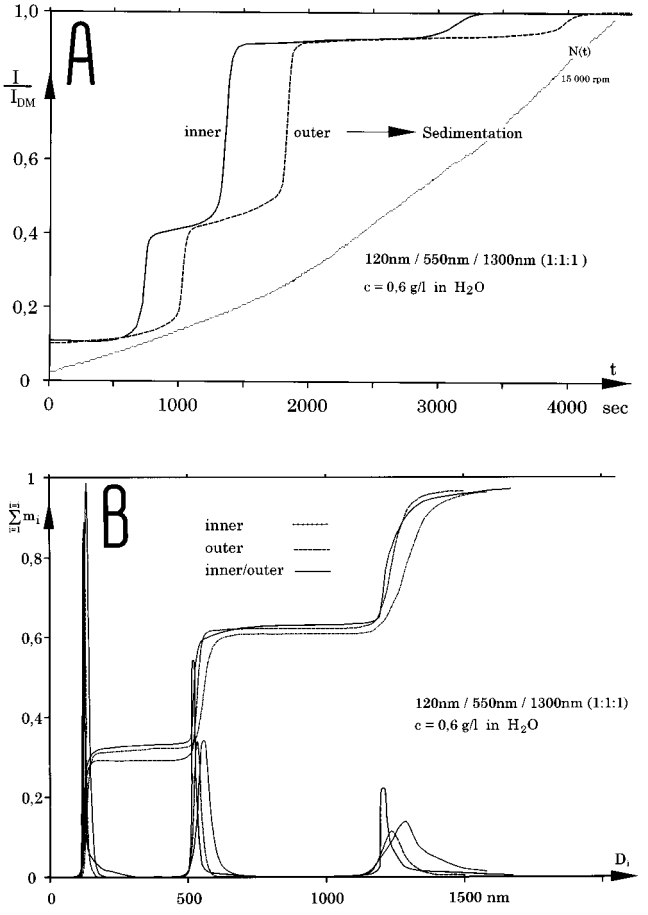

FIGURE 11 (*A*) Two $I(t)$ curves of a mixture of three monodispersed polystyrene calibration latices measured simultaneously with the two-laser-beam setup in an UC. (*B*) Three PSD curves of a mixture of three monodispersed polystyrene calibration latices, calculated from the two $I(t)$ curves in *A* and the difference curve $I(t)_{inner} - I(t)_{outer}$. Both the integral and differentiated curves are shown.

CONCLUSION

Methods for the rapid determination of the PSD of submicron particles by means of a UC are outlined. These are based on turbidity detection and take advantage of an eight-hole rotor to measure seven samples simultaneously. By sweeping the gravitational field, accomplished by raising the rotor speed exponentially from 0 up to 40,000 rpm, good resolution of extremely broadly distributed samples can be completed within 1 h. Both analysis methods, the H_2O/D_2O-analysis and the coupling-PSD technique, employ Stokes' equations and Mie's light-scattering theory. They enable the measurement of the PSD of both very narrow as well as very broadly distributed dispersions with high resolution, as has been demonstrated by several examples. The

new two-laser-beam setup allows 1) an increased range of measurable diameters, 2) increased resolution, and 3) an increase in the number of samples that can be analyzed simultaneously.

REFERENCES

Cantow, H.-J. 1964. Zur Bestimmung von Teilchengrobenverteilungen in der Ultrazentrifuge. *Makromol. Chem.* 70:130–149.

Heller, W., W. J. Pangonis. 1957. Theoretical Investigations on the Light Scattering of Colloidal Spheres. *I. The Specific Turbidity. J. Chem. Phys.* 26:498–506.

Li J., K. D. Caldwell, and W. Mächtle. 1990. Particle characterization in centrifugal fields: comparison between ultracentrifugation and sedimentation field-flow fractionation. *J. Chromatogr.* 517:361–376

Mächtle, W. 1984. Charakterisierung von Dispersionen durch gekoppelte H_2O/D_2O-Ultrazentrifugenmessungen. *Makromol. Chem.* 185: 1025–1039.

Mächtle, W. 1988. Coupling particle size distribution technique. *Die Angewandte Makromol. Chem.* 162:35–52.

Mie, G. 1908. Beitrage zur Optik truber Medien, speziell kolloidaler Metallosungen. *Ann. Phys.* 25:377–445.

Nichols, J. B., E. O. Kraemer, and E. D. Bailey. 1932. Particle size and constitution of colloidal ferric oxide. *J. Phys. Chem.* 36:505–514.

Rowe, A. J. 1992. The concentration dependence of sedimentation. *In* Analytical Ultracentrifugation in Biochemistry and Polymer Science. S. E. Harding, A. J. Rowe, and J. C. Horton, editors. Royal Society of Chemistry, London. 394–406.

Scholtan, W., and H. Lange. 1972. Bestimmung der Teilchengrobenverteilung von Latices mit der Ultrazentrifuge. *Kolloid-Z. u. Z. Polymere.* 250:782–796.